REPORT DOCUMENTATION PAGE

Form Approved
OMB No. 074-0188

1. AGENCY USE ONLY (Leave blank)	**2. REPORT DATE** 1994	**3. REPORT TYPE AND DATES COVERED** Technical report, 1994

4. TITLE AND SUBTITLE
Understanding Satellite Cirrus Cloud Climatologies with Calibrated Lidar Optical Depths

5. FUNDING NUMBERS
N/A

6. AUTHOR(S)
Donald Wylie, Paivi Piironen, Walter Wolf, and Edwin Eloranta

7. PERFORMING ORGANIZATION NAME(S) AND ADDRESS(ES)

Space Science and Engineering Center
University of Wisconsin-Madison
Madison, WI 53706

Department of Meteorology
University of Wisconsin-Madison
Madison, WI 53706

8. PERFORMING ORGANIZATION REPORT NUMBER
N/A

9. SPONSORING / MONITORING AGENCY NAME(S) AND ADDRESS(ES)

SERDP
901 North Stuart St. Suite 303
Arlington, VA 22203

10. SPONSORING / MONITORING AGENCY REPORT NUMBER
N/A

11. SUPPLEMENTARY NOTES
Submitted to The Journal of Atmospheric Sciences, July 1994. No copyright is asserted in the United States under Title 17, U.S. code. The U.S. Government has a royalty-free license to exercise all rights under the copyright claimed herein for Government purposes. All other rights are reserved by the copyright owner.

12a. DISTRIBUTION / AVAILABILITY STATEMENT
Approved for public release: distribution is unlimited

12b. DISTRIBUTION CODE
A

13. ABSTRACT ***(Maximum 200 Words)***

Optical depth measurements of transmissive cirrus clouds were made using coincident lidar and satellite data to improve our interpretation of recent satellite cloud climatologies. These climatologies differ in the way they detect transmissive clouds because some use solar reflectance data (ISCCP) while other use multi-spectral infrared data (CO_2 Slicing). To relate these climatologies and estimate the impact of transmissive clouds on the earth's heat budget, a relationship between visible and infrared radiation properties has to be used. We examined the popular assumption that the ratio of the visible to infrared optical depths should be 2.0 because the visible extinction cross section is twice the infrared absorption cross section when cloud particles re large compared to the wavelength.

14. SUBJECT TERMS
climatology, ISCCP, CO_2 Slicing, lidar optical depth, SERDP

15. NUMBER OF PAGES
39

16. PRICE CODE
N/A

17. SECURITY CLASSIFICATION OF REPORT unclass	**18. SECURITY CLASSIFICATION OF THIS PAGE** unclass	**19. SECURITY CLASSIFICATION OF ABSTRACT** unclass	**20. LIMITATION OF ABSTRACT** UL

NSN 7540-01-280-5500

Standard Form 298 (Rev. 2-89)
Prescribed by ANSI Std. Z39-18
298-102

Appendix C

UNDERSTANDING SATELLITE CIRRUS CLOUD CLIMATOLOGIES WITH CALIBRATED LIDAR OPTICAL DEPTHS

Donald Wylie and Paivi Piironen
Space Science and Engineering Center
University of Wisconsin-Madison
Madison, WI 53706

Walter Wolf and Edwin Eloranta
Department of Meteorology
University of Wisconsin-Madison
Madison, WI 53706

Submitted to
The Journal of Atmospheric Sciences

July 1994

Abstract

Optical depth measurements of transmissive cirrus clouds were made using coincident lidar and satellite data to improve our interpretation of recent satellite cloud climatologies. These climatologies differ in the way they detect transmissive clouds because some use solar reflectance data (ISCCP) while others use multi-spectral infrared data (CO2 Slicing). To relate these climatologies and estimate the impact of transmissive clouds on the earth's heat budget, a relationship between visible and infrared radiation properties has to be used. We examined the popular assumption that the ratio of the visible to infrared optical depths should be 2.0 because the visible extinction cross section is twice the infrared absorption cross section when cloud particles are large compared to the wavelength.

Our lidar-satellite data combination confirmed this relationship for optically thin cirrus ($\tau_{vis} < 1$) that were uniform both vertically and horizontally. Deviations from the 2.0 ratio appeared to come from differences in sampling horizontally variant clouds. The lidar observed a small area ($\doteq$1 m diameter) with the only spatial sampling being from wind advection of the cloud over the sensor while the satellite sensors sampled larger areas 1-20 km in diameter in both the along wind and cross wind directions.

Most cirrus were physically thick (> 1km) and often composed of multiple layers. Super cooled liquid water layers embedded in ice clouds were found in 32% of the cirrus examined.

For thick cirrus and multi-layered cirrus, a direct optical depth comparison was not possible because of the single layer model used in the satellite analysis. However, we simulated what the satellite infrared analysis (CO2 Slicing) would produce in complicated cirrus structures of multiple levels including a super cooled liquid water layer. The simulation used the detailed measurements of vertical extinction from the lidar for deriving the radiances that the satellite would receive on each of its infrared channels. A single cloud height solution was calculated following the CO2 Slicing method. An infrared optical depth was also calculated for this single cloud level using the satellite measured radiances in the 10.8 μm window channel. The calculated cloud level was close to the altitude of the densest cloud layer found by the lidar. The infrared

optical depth (10.8μm) was ≈0.5 of the visible optical depth (0.53 μm) integrated over all the cloud layers which agreed with theory. This indicates that the visible and infrared satellite cloud climatologies derived from can be related for long term studies.

1. INTRODUCTION

Predictions of global warming from the increase of CO_2 in the atmosphere have lacked credibility because of the need to assess the contribution of clouds to the radiation budget (Paltridge, 1980). Cirrus clouds, in particular, have the ability to either offset the CO_2 warming by increased solar reflection or increase the warming by the capture of terrestrial radiation. Thin cirrus in the upper troposphere will add to tropospheric warming because it allows solar insolation while capturing part of the terrestrial radiation. Thick cirrus and multiple layer cloud conditions where water clouds are present under the cirrus produce highly reflective cloud combinations that can lower albedo and solar insolation. Predictions of climate changes ultimately must include the radiative effects of these clouds. However, Stephens et al. (1990) point out that the effect of clouds on the earth's radiation budget is not understood because of the lack of data.

Global cloud and radiation data sets are presently being collected from satellites. The International Satellite Cloud Climatology Project (ISCCP, Schiffer and Rossow, 1983, and Rossow and Schiffer, 1991) has measured cloud cover and radiation for 11 years using the operational weather satellites. Wylie et al. (1994) have studied cirrus clouds from four years of polar orbiting NOAA satellite data, also Woodbury and McCormick (1983) have made a similar analysis of global cirrus from the SAGE II satellite data.

Inter-annual changes in cloud cover have been found. The Wylie et al. (1994) study reported an increase in cirrus with the recent El Nino-Southern Oscillation (ENSO) that began in 1991. A similar change in cloud cover in the 1982-83 ENSO was also found by Weare (1992) using the NIMBUS 7 data set. These studies indicate that cloud cover is linked to climatic fluctuations.

Estimates have been made of the effect of lower tropospheric clouds on the earth's heat budget by Tselioudis et al. (1993) using ISCCP data, but similar calculations for upper tropospheric clouds have not been attempted because of the complications of estimating the effects of both the visible and the infrared radiative processes together. Boundary layer and lower tropospheric clouds affect solar insolation but have little effect on infrared cooling, while cirrus clouds affect both radiative processes. Satellite observations have usually been restricted to either the visible or the infrared. The satellite data used by Wylie et al. (1994) and Weare (1992) were from longwave infrared sensors, therefore the effect on solar radiation will have to be estimated since it was not measured. The ISCCP differs from these two studies in that it employs visible sensors for detecting transmissive cirrus clouds. The IR contribution must be estimated from the visible reflectance measurements. The 11 year record of the ISCCP (Schiffer and Rossow, 1983) will allow studies of fluctuations of cloud cover with many short term climate changes including three ENSO's. The SAGE II data set can also be used for deriving visible optical depths (Laio, et al. 1994a and b). These satellite data sets are complimentary where they overlap, but the overlap is small, about one year for each intersection. To study interannual changes, trends, and longer term fluctuations, each of these data sets will have to be used separately. Visible to infrared radiance relationships will have to be used to fully estimate the effect of cirrus changes on heat budget parameters.

Our knowledge about the relationship of the solar reflection to the infrared attenuation in cirrus clouds is limited. For particles which are large compared to the wavelength, we expect the visible scattering cross section to be twice the infrared absorption cross section when there is little visible absorption and strong infrared absorption by ice and liquid water. This implies that the ratio of the visible to the infrared optical depth should be about 2.0. Modelling of the radiative properties of ice crystals by Minnis et al. (1993) and Mitchell and Arnott (1994) support this assumption. However, variances in cloud particle size and shape could vary this ratio from 1.8 to 4.0.

In situ measurements of cirrus microphysical properties have found extremely large variances in number density, ice-water content and particle size (Dowling and Radke, 1990). The number density of cloud particles varies by 8 orders of magnitude, from 10^{-4} L^{-1} to 10^{+4} L^{-1}. The ice-water content varies over 10 g m^{-3} and the particle size can vary from 1 to 8000 μm. With this wide range of possible microphysical variances, large variances in the radiative properties are expected.

Few measurements of cirrus have been made when data from both the visible and IR were collected simultaneously. Platt (1979) used a vertically pointing IR radiometer with a visible lidar to study a limited number of thin cirrus cases. Minnis et al. (1990) studied one case from FIRE-I (the First ISCCP Regional Experiment in October 1986) using infrared data from a satellite and visible data from a lidar. Platt (1979) found a visible to IR optical depth ratio of 2.0 while Minnis' case was slightly higher at 2.1. These cases were mostly thin single layer cirrus.

To use the global cloud climatologies, we need to understand what has been measured and how their representation of clouds depicts the radiative transfer in both the visible and the infrared. The retrieval of cloud parameters in the satellite climatologies has been based on the assumption that the clouds are a single thin layer and that they cover the Field of View (FOV) of the satellite sensor for each pixel in the image. ISCCP and Wylie et al. (1994) only solved for one cloud level in each pixel (FOV). A comparison of satellite cloud retrievals to ground based National Weather Service observations over the continental United States found that low and middle tropospheric clouds were present in 52% of the cases where the satellite cloud detection system found an upper tropospheric cloud (Menzel et al., 1992). Similar statistics on the frequency of multiple cloud layers over oceans are shown in Hahn et al. (1982). Lidar data collected at the University of Wisconsin-Madison (Figure 1) found that cirrus are often geometrically thick reaching depths up to 5 km. Thus, we expect that cirrus are more complicated than the assumed thin single layer model used in the cloud retrieval algorithms.

Because of the uncertainty of what satellite cloud retrievals represent and the need to relate the different climatologies so that longer cloud records can be compiled, we collected a data set of high quality lidar observations with coincident satellite data. The purpose of this study is twofold: 1) to asses the applicability of the "single thin layer" assumption used in satellite cloud retrievals, and 2) to asses the validity of the 2.0 visible to infrared optical depth ratio so the satellite cloud climatologies can be combined for a more complete assessment of radiative transfer processes.

2. MEASUREMENT TECHNIQUE

This study was initiated in 1989 using the unique measurement systems at the University of Wisconsin-Madison (Ackerman, et al., 1993). Visible optical depths of cirrus were obtained from the High Spectral Resolution Lidar (HSRL) while infrared optical depths were obtained from satellite data so that the information collected could be related to the cirrus climatologies of Wylie et al. (1994) and ISCCP.

2.a. The HSRL

In order to make reliable measurements of the extinction profile, the HSRL measures two signals from the 0.53 μm transmitted pulse which can be processed to yield separate lidar returns for aerosol and molecular scattering. This separation is possible because the spectrum of the molecular lidar return is Doppler broadened by the thermal motion of the molecules while the slow moving aerosol particles generate negligible spectral broadening. The molecular scattering cross section is a function of molecular density and can be calculated from Rayleigh scattering theory and an independently measured temperature profile. The HSRL then uses molecular scattering as a calibration target which is available at each point in the lidar return.

Two lidar returns are derived; these are given by the following equations for the signal power received from molecular scattering, $P_m(r)$, and aerosol scattering, $P_a(r)$:

$$P_m(r) = E_o \frac{cA_r}{2r^2} \beta_m(r) \frac{3}{8\pi} exp(-2\tau(r)) \tag{1}$$

$$P_a(r) = E_o \frac{cA_r}{2r^2} \beta_a(r) \frac{P(\pi,r)}{4\pi} exp(-2\tau(r)) \tag{2}$$

E_o = Laser pulse energy, J.
c = Speed of light, ms^{-1}.
A_r = Collecting area of the receiver, m^2.
r = Range to the scattering volume, m.
β_a = Aerosol scattering cross section per unit volume, m^{-1}.
β_m = Scattering cross section per unit volume for air molecules, m^{-1}.
$\frac{P(\pi,r)}{4\pi}$ = Backscatter phase function, sr^{-1}.
τ = Optical depth.

Equation 1 contains two unknowns: the optical depth between the lidar and the scattering volume, $\tau(r)$, and the molecular scattering cross section, $\beta_m(r)$. Molecular scattering is described by the Rayleigh scattering equation and is directly proportional to atmospheric density, $\rho(r)$.

$$\beta_m(r) = C\rho(r)$$

Thus if we define a range-squared, energy corrected molecular lidar return:

$$S_m(r) = P_m(r)r^2/E_o$$

$$ln[S_m(r)] = constant + ln[\rho(r)] - 2\tau(r)$$

The optical depth between any two ranges, r and r_o, is given by:

$$\tau(r) - \tau(r_o) = 0.5\, ln[\rho(r)/\rho(r_o)] - 0.5 \ln[S_m(r)/S_m(r_o)] \tag{3}$$

The average extinction cross section in a layer between r_o and r can be computed from equation 3:

$$\overline{\beta_e(r,r_o)} = [\tau(r) - \tau(r_o)]/[r-r_o] \tag{4}$$

More details can be found in Grund and Eloranta (1991) and Piironen and Eloranta (1994).

2.b. Satellite Infrared

The satellite cloud analysis of Wylie et al. (1994) assumes that the radiative effects of the clouds occur at only one level in the troposphere. This allows a simple calculation of cloud emittance at 10.8 μm, the longwave window channel, from the radiances measured by the satellite in the cloudy pixel (R_{sat}), a clear pixel (R_{clr}), and the radiance expected if an opaque cloud were present at the pixel (R_{cld}).

$$\epsilon_{ir} = [R_{clr} - R_{sat}] / [R_{clr} - R_{cld}] \tag{5}$$

R_{sat} was measured from the pixel that covered the HSRL while R_{clr} is an estimate of the radiance that would have been measured if the cloud was not present. This clear radiance estimate was derived from the nearest clear pixel by assuming that the background under the cloud was the same as at the location where R_{clr} was taken. R_{cld} was calculated from the temperature of the mid-cloud level using rawinsonde data from Green Bay, WI which was the nearest sounding to the

HSRL. To simplify the calculation, the black body temperature to the fourth power (T^4) was used in place of R. The satellite measurements are calibrated to both radiance (R) and blackbody temperature (T). Equation 5 was expressed as:

$$\epsilon_{ir} = [T^4_{clr} - T^4_{sat}] / [T^4_{clr} - T^4_{cld}] \tag{6}$$

where:

T_{clr} = blackbody brightness temperature for a clear pixel
T_{sat} = blackbody brightness temperature for a cloudy pixel
T_{cld} = the air temperature at the mid-cloud height.

The mid-cloud altitude was determined from the appearance of the cloud on the HSRL backscatter vertical profile. This approximated the cloud level that the HIRS analysis reports for transmissive clouds (Wylie and Menzel, 1989).

IR optical depths were calculated from the emittances assuming no scattering at the window channel IR wavelength (10.8 μm) and that transmission was the compliment of emission:

$$\tau_{ir} = -ln(1-\epsilon_{ir}) \tag{7}$$

The infrared optical depths were also corrected for the angle of the satellite scan through the atmosphere using the cosine of the zenith angle.

3. DATA

HSRL data were examined for 21 separate days covering all four seasons (see Table 1). NOAA 12 overpasses of Madison, WI were available when most of the HSRL data were taken. However, on six days, GOES 7 data were compared to the HSRL because of the absence of NOAA 12 data. Comparisons were restricted to cases with visible optical depths < 3 when the HSRL probed through the entire cloud. Total cloud penetration was determined by the presence of molecular backscatter signal beyond the cloud top (Equation 1).

4. RESULTS

4.a. Visible and IR Optical Depths

To compare visible and infrared radiative properties, satellite infrared optical depths from Equation 7 were plotted with the HSRL visible optical depths from Equation 3 (see Figure 2). The 21 cases covered a variety of transmissive cirrus situations. The clouds were separated into three classes: 1) geometrically thin, covering < 2.5 km, 2) geometrically thick, covering > 2.5 km, and 3) multi-layered clouds. Many of the multiple level cloud cases included a thin layer of super cooled liquid water (distinguished by low values of depolarization measured by the HSRL) and often included ice crystals precipitating from the layer. Liquid water layers embedded in cirrus were found on 32% of the days that the HSRL collected cirrus data.

Error estimates for both the HSRL and satellite optical depth measurements are also included in Figure 2. For the visible optical depth (horizontal bars) the error was computed from an error analysis including photon counting statistics, error in the observed density profile, and error in system calibration. For the satellite infrared optical depths (vertical bars), the error was estimated by assuming a 2 K error in each variable in Equation 6. This is our estimate of the maximum uncertainty in determining the clear radiance (T^4_{clr}) and the cloud level radiance (T^4_{cld}). The largest source of clear radiance error was spatial variances or gradients in the land surface or low level aerosol density between the locations of the HSRL and where T_{clr} was obtained. The largest source of T_{cld} error was the air temperature gradient between the location of the HSRL and the rawinsonding. The satellite radiometric measurements are calibrated to 0.8 K which is a far better accuracy than the other error sources. The location of the HSRL in the satellite images was also determined to an accuracy of < 1 pixel using navigation adjustments from rivers and lake shorelines.

4.b. Single Layer Cirrus

An example of a single layer cirrus cloud is shown in Figure 3 from 26 October 1993. The cirrus cloud was found between 9 and 11 km and was fairly uniform in the vertical dimension and in time as seen in the lidar time section. The NOAA satellite image (Figure 4) also showed very uniform conditions around the HSRL (black dot on the image). Brightness variations around the

HSRL were highly enhanced but span a range of only 1.5 K in blackbody temperature. The cirrus over the HSRL was part of a large air mass moving from the southwest to the northeast. The visible optical depth was 0.5 at the time of the NOAA overpass (0:30 UT). The satellite infrared optical depth was found to be 0.28, yielding a τ_{vis}/τ_{ir} ratio of 1.8, close to the expected 2.0.

Low level aerosols were also present from 0-3.2 km as indicated by the HSRL (Fig. 3). These aerosols were probably not included in the satellite optical depth measurement. T_{clr} in Equation 5 was taken from an area 150 km to the southeast in the satellite image where similar low level aerosols should have been present.

4.c. The Effects of Multiple Cloud Layers

Multiple layers of clouds have been very common during this study. Five cases of multiple layers were examined in this study. One example is shown in Figure 5 for 11 November 1993 when the cirrus was changing during the HSRL observation. Initially, only one layer of cirrus from 7 to 10 km was present; then at 1:15 UT a second layer appeared. Depolarization measurements by the HSRL indicated that the intense backscatter levels (solid white) were liquid water particles while the rest of the cloud was ice. Visible optical depths increased from 0.4-0.6 to 1.0 at the NOAA overpass at 1:30 UT. After 1:40 UT the visible optical depth exceeded 3.0, the maximum measurable by the HSRL. The NOAA 12 IR image in Figure 6 also shows this change as dense clouds moved in from the west. Notice that the light cirrus to the east (down wind) has faint northwest-southeast striations while the denser area to the west (up wind) has orthagonal southwest-northeast striations. Both patterns are skewed to the westerly wind.

The water layer dominated the optical depth of the combined cirrus layers. The upper ice cloud maintained a nearly constant optical depth of 0.4-0.6 until 01:40 UT when the HSRL could no longer penetrate through the water layer.

The satellite measured blackbody radiance decreased from 261 K before the lower layer formed (to the east in the image), to 253 K at the HSRL location. In the dense two layer cloud it dropped to 243 K at 30 km west of the HSRL in the image.

Simulations of the HIRS radiance and cloud height measurements were made for three situations: 1) the single layer case, 2) the two layers at the NOAA 12 over pass at 1:30 UT, and 3) the point when the lower water layer first obscured the HSRL at 1:40 UT. The second and third situations represent problems to the basic assumption used in satellite cloud retrievals - the single level description of the cloud. The expected response of the multi-spectral HIRS cloud retrieval algorithm used by Wylie et al. (1994) to multi-layered clouds is that it would place the single cloud height between the two layers (Wielicki and Coakley, 1981 and Menzel et al., 1992). The single level cloud height is calculated from the mean altitude of infrared radiative divergence, similar to a center of mass concept in kinematics. However, when one cloud layer has more optical depth than the other, the multi-spectral HIRS cloud height solution is expected to move toward the denser layer. An exception to this trend occurs when the top layer is nearly opaque and obscures the view of the lower layer, forcing the HIRS solution into the top layer.

Attempts have been made to extract more than one cloud level from the multi-spectral HIRS data. However, the solution of the radiative transfer model for the HIRS sensors requires the integral of the radiation over a broad portion of the troposphere. The cloud height solution has been mis-labelled the CO2 Slicing Method from the desire that each channel would see a different "slice" of the atmosphere; however, altitude sensitivities of the channels are broad and overlap. Each HIRS channel receives radiation from 3-5 km of the troposphere. To solve for more than one cloud level, the vertical profile of the clouds must be determined. Since each HIRS sensor sees the integral of the radiation over a large depth of the troposphere, a wide variety of cloud structures could be present from which no unique solution can be made. The only tractable solution for the HIRS data is one cloud level.

The response of the multi-spectral HIRS algorithm to the cloud structures observed by the HSRL was simulated by calculating what the HIRS channels should have seen given the temperature structure and the infrared emittance and transmittance of each cloud layer. HIRS data were available for all cases where the NOAA satellites were used. The HIRS data were not used because the HIRS data were not directly over the HSRL. The HIRS pixels (FOV) do not overlap and contain gaps between pixels that are about the same dimensions as the FOVs. For accurate comparisons to the HSRL, radiative data must come from the location of the HSRL. Spatial variance of the clouds can cause large errors. These errors are discussed in detail in section 4d.

The radiance received by each HIRS sensor was estimated using a simple model of three cloud layers.

$$
\begin{aligned}
I_i = {} & \int_{p1}^{0} B[i,T(p)]\{dS_i(p)/dp\}dp + S_i(p1)\epsilon_1 B[i,T(p1)] \\
& + (1-\epsilon_1)\Big[\int_{p2}^{p1} B[i,T(p)]\{dS_i(p)/dp\}dp + S_i(p2)\epsilon_2 B(i,T(p2))\Big] \\
& + (1-\epsilon_1)(1-\epsilon_2)\Big[\int_{p3}^{p2} B[i,T(p)]\{dS_i(p)/dp\}dp + S_i(p3)\epsilon_3 B(i,T(p3))\Big] \\
& + (1-\epsilon_1)(1-\epsilon_2)(1-\epsilon_3)\Big[\int_{psfc}^{p3} B[i,T(p)]\{dS_i(p)/dp\}dp + S_i(sfc) B(i,T(sfc))\Big]
\end{aligned}
\qquad (8)
$$

Where:

$B[i,T(p)]$ = the Planck function for spectral channel (i) and temperature $T(p)$,
$S_i(p)$ = the transmittance of that radiation from level p through the atmosphere,
ϵ_x = the emittance for cloud layer x.

The emittance (ϵ) for each cloud layer was approximated from the HSRL measurements of the visible optical depth of the layer. The infrared optical depth was assumed to be one half of the visible optical depth for each cloud layer and the emittance (ϵ) was derived from Equation 7.

The approximated radiances for the HIRS channels were used in the algorithm described by Wylie et al. (1994) for determining a single cloud level. This cloud level was then used for determining T_{cld} from the rawinsonde data. With a new T_{cld} and the measured T_{sat} and T_{clr}, Equations 6 and 7 were re-applied to give an estimate of what the HIRS algorithm would have derived for the cloud altitude and infrared optical depth (τ_{ir}). Note that this calculation used a combination of satellite measured radiances, T_{sat} and T_{clr} and a new radiance for the approximate single cloud level, T_{cld}.

The first situation on 11 November, was a single cirrus layer with a mean height of 8.5 km. The infrared optical depth calculated from Equations 5 and 6 was 0.25. With the HSRL visible optical depth measurement of 0.5, the τ_{vis}/τ_{ir} ratio of 2.0 agreed with theory.

The HIRS radiances for the second situation at 1:30 UT were calculated from Equation 8 using two cloud levels at 5 and 8.5 km. The visible optical depths of the two layers measured by the HSRL were 0.9 (lower) and 0.6 (upper). Emittances of 0.4 for the lower layer and 0.3 for the upper layer were calculated from Equation 7 by assuming that the infrared optical depths were one half of the visible HSRL measurements. The single cloud layer calculated from the Wylie et al. (1994) algorithm was 6.6 km which was between the two cloud layers. The infrared optical depth from this level and the AVHRR T_{sat} and T_{clr} measurements was 0.6. Using the HSRL measured visible optical depth of 1.0, τ_{vis}/τ_{ir} was 1.7, slightly lower than theory.

In the third situation at 1:40 UT the total optical depth exceeded the HSRL measurement capability. However, Equation 8 was employed to estimate HIRS radiances by assuming that the upper cloud layer remained at the same optical depth as measured at 1:30 UT and the lower cloud layer was at the level of HSRL saturation, 3.0 visible or 1.5 infrared. The single cloud level solution was 5.9 km, 0.7 km closer to the liquid water layer than the calculation from the second situation.

This is an example of how the HIRS single cloud level solution used by Wylie et al. (1994) responds to multiple level clouds. The technique is constrained to reporting only one cloud layer. For one layer of transmissive cirrus, it places the cloud level near the center of the layer as predicted by Wielicki and Coakley (1981). Similar results for a previous comparison with lidar data were reported in Wylie and Menzel (1989). For two layers, the HIRS solution was between the layers, moving toward the denser lower layer as it became the dominant layer.

We acknowledge that the estimation of HIRS infrared radiances and the calculation of infrared optical depths for the two layered cloud appears to be a circumlocution because HSRL visible optical depth measurements were used. However, the infrared optical depth calculation (Equations 6 and 7) involves more than the cloud height and the radiance (T^4_{cld}) from this cloud height level using the temperature sounding. The other terms in Equation 6, T_{sat} and T_{clr}, came from satellite measurements independently of the HSRL measurements. Also, Equation 8 uses radiances from the sounding (the integrals) as well as the emittances of the cloud layers that came from the HSRL optical depths. To test the sensitivity of Equation 8 to the method of transforming HSRL visible optical depth measurements to infrared emittances, the calculations were repeated using τ_{vis}/τ_{ir} ratios of 1.0 and 4.0 on the HSRL visible optical depth measurements. These two tests differed from the original relationship by a factor of 2. These tests changed the single cloud level solution by ±0.6 km and the derived infrared optical depth by ±0.1. This is smaller than the changes caused by the increase in density of the lower cloud layer.

4.d. The Effects of Vertical and Horizontal Variability

Most of the deviations from the 2.0 visible to IR optical depth ratio in Figure 2 came from cirrus clouds with high horizontal variations. An example of such a cloud observed with the HSRL on 2 September, 93 is shown in Figure 7. The NOAA 12 satellite image from the 01:36 UT overpass (Figure 8) shows a small and long cirrus cloud which is partially over the HSRL (dot in the image). This cloud moved east on a 75° bearing. Only part of it crossed the HSRL. Larger clouds up wind crossed the HSRL at 01:55 UT. This is an example of how spatial variability affected the lidar-satellite comparison. The visible optical depth at the time of the satellite overpass was 0.2 while the infrared optical depth at the presumed HSRL location was 0.05 yielding a τ_{vis}/τ_{ir} ratio of 4.0, larger than predicted from theory. The satellite radiance was taken in a gradient region where any error in location could raise or lower its value. Also, for horizontally small and narrow clouds, the larger size of the satellite radiometer's FOV may have averaged more cloud area with less cloud optical depth than that viewed by the HSRL.

Most of the low optical depth cases shown in Figure 2 came from GOES satellite data which has a larger FOV than the AVHRR (10.8 km diameter GOES vs. the 1 km AVHRR). The GOES tended to find higher optical depths than predicted by the lidar, the opposite of the 2 September case previously discussed. Substantial horizontal variances were present in all of the cases with visible optical depth < 0.2. We suspect that the satellite pixels used to determine clear radiances (T^4_{clr}) may have had cloud contamination and thus T^4_{clr} may have been too cold which would cause higher infrared optical depths to be calculated.

Another example of a variable cloud situation was found on 15 April, 94, see Figures 9 and 10. The HSRL image of backscatter cross section (Figure 9) showed large variations in the optical depth with time while the NOAA 12 AVHRR image (Figure 10) showed cirrus clouds with a variety of shapes. An elongated cloud partially covered the HSRL at the time of the satellite overpass (00:49 UT) and moved toward the northeast on a 80° bearing. There were at least two layers of cirrus as indicated in Figure 9. The lower layer was more dense but highly variable in nature and contained some super cooled water. The upper layer was very thin and composed entirely of ice. The visible optical depth was 0.75 while the infrared was 1.07. This combination produced a τ_{vis}/τ_{ir} optical depth ratio of 0.7, far less than the theoretical 2.0.

To statistically estimate the errors of FOV size differences and possible miss-registration of the satellite image, data from the Volume Imaging Lidar (VIL) were examined. This is a 1064 nm Nd:YAG lidar with an optics system that scans from horizon to horizon. It was operated on 1 December, 1989 for two hours when transmissive cirrus were present. The VIL performed a pair of scans in 2 minute cycles. The cycle consisted of a cross wind scan (north to south) followed by an along the wind scan (east to west). Examples of images made from these scans are shown in Figures 11 and 12. The cross wind scans are the upper panel and the along wind scans are the lower panel.

The two hour period from 19:30 to 21:30 UT (13:30 to 15:30 CST) began with light broken cirrus to the north and one line of precipitating cirrus to the south (see Fig. 11). The cirrus to the north were in small patches at a variety of levels from 6.5 to 9 km in altitude. Light virga were observed. One large contrail appeared at 7.7 to 8.5 km altitude, 15 km south of the VIL (center point). A dense line of precipitating cirrus was also found 30 to 43 km south of the VIL. Later (1.25 hours) dense cirrus moved over the VIL (Fig. 12). A nearly continuous cloud from 6.5 to 9.3

km altitude was present within most of the range of the VIL. Some optically dense layers were found at 7 and 9 km.

To quantify the effects of cloud spatial variability on scanning method and FOV size, the backscatter measured by the VIL was vertically integrated from the series of slant angle scans in each cross section. Although the backscatter to extinction relationship may not be simple, we can assume that the backscatter is nearly linearly related to extinction for these optically thin clouds. The vertical integral of backscatter through the cloud is proportional to the optical depth of the cloud when the optical depth is small. The effect of this simplication is that the optical depth structural variations are most likely larger than the backscatter structural variations that are shown in Figures 13 and 14.

The cross wind scans were used to describe the areal structure of the cloud. Wind advection through each scan implied that the clouds were sampled at approximately 3 km intervals. Since the VIL cross sections have 100 m resolution along the scan, the cloud volume was sampled with a resolution of 0.1 x 3 km.

To estimate the effects of cloud structural variance on the averaged vertically integrated backscatter, two spatial averages were made. One average was made from the cross wind scans using wind advection to represent the satellite's spatial sampling. The other average was made from the along wind scans to represent the sampling of a vertically pointing lidar that uses wind advection for cloud sampling. Each average was constructed for simulated satellite FOV diameters of 1, 4, 8 and 20 km. The along wind scans have only the width of the lidar beam (< 1 m) and thus the average is a line sample. The difference between these two averages of vertically integrated backscatter was used to approximate the sampling error between the satellite and stationary lidar sensors. This error is expressed as a fraction of the along wind lidar average in Figures 13 and 14. To estimate the possible error from mis-registration of the satellite image, the cross wind sampled segment was shifted from the center position of the VIL, see Figures 13 and 14.

The error between line and areal averaged measurements is the left most point in Figures 13 and 14. This error ranged from 5 to 29%. It was higher for the light and scatter cirrus simulating a 20 km FOV (Figs. 11 and 13) than the smaller simulated FOVs and the denser cirrus (Figs. 12 and 14). In the denser cirrus, the line vs. area sampling error ranged from 20 to 25 % (Fig 14).

The misalignment test shows that the area-line error increases with cross wind misalignment. The light cirrus (Fig. 13) have very large errors because of the spacing between cirrus features of 12-20 km and close alignment of the structures with the direction of the wind. The error or difference from the cross wind average often exceeded the along wind average (error > 100 %). These errors were smaller in the denser cirrus (Fig. 14). Operational satellites have typical image registration errors of 12 to 20 km. A 12 km misalignment when compared to a ground based sensor can cause an error of 50 % or greater. For larger FOV sizes of 8 and 20 km, this error decreases slightly. Because of this problem, special effort was made to align the satellite images to a one pixel accuracy.

5. DISCUSSION

In general, our observations of cirrus conformed to the expected relationship of the visible optical depth being twice the infrared optical depth. The scatter around the $\tau_{vis}/\tau_{ir} = 2.0$ optical depth ratio mostly came from the differences between the lidar and satellite methods of probing the clouds. The high spatial variability of the clouds and the difficulty of evaluating small optical depths from satellite imagery were found to be the largest sources of error in this comparison. The thin line sampling of the HSRL vs. the areal scan of the satellite sensors could cause differences of 20-25% in measurements of the same variable. Any mis-registration of the location of the HSRL in the satellite image caused potentially larger errors and had to be corrected in this study. The initial evaluation of the HSRL and satellite data had more scatter than shown in Figure 2. This gave the impression that variations in cloud structure and microphysical content were causing variations in the visible-infrared optical depth relationship. Re-analysis of the data with an intensive effort to remove location uncertainties reduced the scatter in Figure 2.

The satellite measurement of τ_{ir} for optically thin clouds also had a bias because of the way in which the numerator of Equation 6 (T^4_{clr}-T^4_{sat}) was evaluated. This required a measurement of the difference between the clear and cloudy radiances in the satellite image. For optically thin clouds, variations in the underlying land surface were of nearly the same magnitude as (T_{cld}-T_{sat}). The precision and noise characteristics of the satellite sensors require that the numerator terms in Equation 6 be at least 0.8 K different (T_{clr}-T_{sat} > 0.8K) for the cloud to be distinguished on the satellite image. This forces a minimum of 0.03-0.05 for τ_{ir}. Any error in the terms in Equation 6 from spatial variance tend to increase τ_{ir} because errors that would reduce τ_{ir} make cloud detection impossible. This is possibly why 7 of the 9 points in Figure 2 with $\tau_{vis} < 1$ appear above the 2.0 line. It also indicates that the minimum optical depth (infrared) detectable in a satellite image is about 0.05.

Optically thin cirrus ($\tau_{vis} < 1$) best conformed to the assumption made by most satellite cirrus cloud detection algorithms that cirrus clouds can be described as a single thin layer even though they span depths of 1-3 km. This assumption is possible when the clouds have little vertical variance in radiative properties.

For dense cirrus with optical depths $\tau_{vis} > 1$ ($\tau_{ir} > 0.5$), the cirrus were often over 3 km thick and in two or more layers. Vertical variations in optical density were common and liquid water layers were often present inside the ice clouds. The retrieval of a single cloud layer from the HIRS data to describe the infrared characteristics of these clouds appears to work as a first approximation of infrared divergence. More detail in the vertical would be helpful for the development of radiative transfer models. But the fact that the infrared optical depth calculated from the single cloud level solution followed the theoretical relationship of being nearly one half of the visible optical depth is very useful for inter-relating cloud climatologies. Development of radiative transfer algorithms for global numerical models requires global data sets on clouds and their radiative properties. Satellites are currently the best source of this data.

We found super cooled liquid water layers in 32% of the 48 cirrus cases measured by the HSRL which was more frequent than we expected. These case include an extra 25 days which were not analyzed with satellite data. This data set may not be large enough to state the frequency of liquid water in all cirrus clouds. The HSRL was operated mostly during NOAA 12 overpasses at dusk and after dusk. Cirrus data could only be obtained when obstructions from lower water clouds were not present or minimal enough to permit the view of the cirrus. Cirrus (ice clouds) obviously exist above low altitude liquid water clouds but we have little data from these cirrus because of low cloud obscurations.

6. CONCLUSIONS

The assumption of a single cloud level used by the satellite cloud climatologies is applicable to a large portion of the satellite data. The manner in which optical depths are calculated from the 10.8 μm window channel measurements appears to approximate the vertically averaged optical depths for a variety of cloud structures which are far more complicated than one layer.

The cirrus climatologies derived from different satellite data, visible and infrared 10.8 μm window, can be related using the 2.0 optical depth ratio to form longer records of cirrus cloud cover and describe inter-annual changes. This work is needed to asses the relationship of cirrus clouds to climatic changes and their role in the earth's heat budget. This study used clouds of visible optical depths ranging from 0.25 to 3.0. According to Wylie et al. (1994), these clouds cover 32% of the earth which is a significant part of the earth's cloud cover.

Super cooled liquid water layers are common inside ice clouds and can easily change the radiative characteristics of these clouds. They were found in nearly one third of our cirrus data. Their impact on radiative processes needs to be evaluated and models of radiative processes in clouds need to include them.

The problem of matching point or line sensors (lidars) to areal scanners (satellites) is an obstacle to field programs and the use of their data with global cloud climatologies. Miss-matches in sampling and scanning can lead to large errors when data sets are compared and these errors can be mistaken for variances in radiative properties of the clouds. Scanning sensors and a large number of cases are needed from these field programs to define cloud radiative properties.

7. REFERENCES

Ackerman, S. A., E. W. Eloranta, C. J. Grund, R. O. Knuteson, H. E. Revercomb, W. L. Smith and D. P. Wylie, 1993: University of Wisconsin Remote Sensing Pilot Experiment. Bull. A.M.S., **74**, 1041-1049.

Dowling, D. R., and L. F. Radke, 1990: A summary of the physical properties of cirrus clouds., J. Appl. Meteor., **29**, 970-978.

Grund, C. J. and E. W. Eloranta, 1991, University of Wisconsin high spectral resolution lidar., Optical Eng., 30, 6-12.

Hahn, C. J., C. S. Warren, J. London, R. M. Chervin and R. Jenne, 1982: Atlas of simultaneous occurrence of different cloud types over the oceans., NCAR Tech. Note NCAR TN-201+STR, National Center for Atmospheric Research, Boulder, CO, 212 pp.

Klett, J. D., 1980: Stable analytical inversion solution for processing lidar returns., Appl. Optics, **20**, 211-220.

Laio, X., W. B. Rossow, and D. Rind, 1994a: Comparison between SAGE II and ISCCP high-level clouds, Part I: Global and zonal mean cloud amounts., submitted to J. Geophy. Res.

______b: Comparison between SAGE II and ISCCP high-level clouds, Part II: Locating cloud tops., submitted to J. Geophy. Res.

Menzel, W. P., D. P. Wylie, and K. I. Strabala, 1992: Seasonal and diurnal changes in cirrus clouds as seen in four years of observations with the VAS., J. Appl. Meteor., **31**, 370-385.

Minnis, P., D. F. Young, K. Sassen, J. M. Alvarez and C. J. Grund: 1990: The 27-28 October 1986 FIRE IFO Cirrus Case Study: Cirrus parameter relationships derived from satellite and lidar data., Mon. Wea. Rev., **118**, 2402-2425.

Minnis, P., K. N. Liou and Y. Takano, 1993: Inference of cirrus cloud properties using satellite-observed visible and infrared radiances. Part I: Parameterization of radiance fields., J. Atm. Sci., **50**, 1279-1304.

Mitchell, D. L. and W. P. Arnott, 1994: A model predicting the evolution of ice particle size spectra and radiative properties of cirrus clouds. Part II: Dependence of absorption and extinction on ice crystal morphology., J. Atm. Sci., **51**, 817-832.

Paltridge, G. W., 1980: Cloud-radiation feedback to climate., Quart. J. R. Met. Soc., **106**,895-899.

Piironen, P. and E. W. Eloranta, 1994: Demonstration of high-spectral-resolution lidar based on an iodine absorption filter., Optics Letters, **19**, 234-236.

Platt, C. M. R., 1979: Remote sounding of high clouds: I. Calculation of visible and infrared optical properties from lidar and radiometer measurements., J. of Appl. Meteor., **18**, 1130-1143.

Rossow, W. B. and A. A. Lacis, 1990: Global and seasonal cloud variations from satellite radiance measurements. Part II: Cloud properties and radiative effects., J. Climate, **3**, 1204-1253.

Rossow, W. B., and R. A. Schiffer, 1991: ISCCP cloud data products., Bull. Am. Meteor. Soc., **72**, 1-20.

Schiffer, R. A., and W. B. Rossow, 1983: The International Cloud Climatology Project (ISCCP): The first project of the World Climate Research Programme., Bull. Am. Meteor. Soc., **64**, 779-784.

Shipley, S. T., D. H. Tracy, E. W. Eloranta, J. T. Trauger, J. T. Sroga, F. L. Roesler, and J. A. Weinman, 1983: High spectral resolution lidar to measure optical scattering properties of atmospheric aerosols. 1: Theory and instrumentation., Applied Optics., **23**, 3716-3724.

Stephens, G. L., S. C. Tsay, P. W. Stackhouse, and P. J. Flatau, 1990: The relevance of the microphysical and radiative properties of cirrus clouds to climate and climatic feedback., J. Atm. Sci., **47**, 1742-1753.

Tselioudis, G., W. B. Rossow and D. Rind, 1992: Global Patterns of cloud optical thickness variation with temperature., J. of Climate., **5**, 1484-1497.

Weare, B. C., 1992: Variations in Nimbus-7 cloud estimates. Part I: Zonal averages., J. Climate, **5**, 1496-1505.

Wielicki, B. A., and J. A. Coakley, 1981: Cloud retrieval using infrared sounder data: Error analysis., J. Appl. Meteor., **20**, 157-169.

Woodbury, G. E., and M. P. McCormick, 1983: Global distributions of cirrus clouds determined from SAGE data., Geophy. Res. Letters, **10**, 1180-1183.

Wylie, D. P. and W. P. Menzel, 1989: Two years of cloud cover statistics using VAS. J. Clim. Appl. Meteor., **2**, 380-392.

Wylie, D. P., W. P. Menzel, H. M Woolf and K. I. Strabala, 1994: Four years of global cirrus cloud statistics using HIRS., J. Climate, in press.

TABLE 1: The dates and times of the satellite-lidar comparisons.

Month/Date/Year	Time	Satellite	
08/24/93	01:30 UTC	NOAA 12	Multiple layers
09/02/93	01:37	NOAA 12	Thin and variable
09/08/93	01:08	NOAA 12	Multiple layers
09/09/93	00:46	NOAA 12	Thick cirrus
10/02/93	00:51	NOAA 12	Thick cirrus
10/12/93	00:36	NOAA 12	Thin
10/25/93	00:57	NOAA 12	Thin and variable
10/26/93	00:35	NOAA 12	Uniform layer
10/28/93	01:32	NOAA 12	One thick layer
11/10/93	00:12	NOAA 12	Two layers
11/11/93	01:31	NOAA 12	Two layers
02/04/94	00:06, 00:36, 01:06 and 01:36	GOES	One thick layer
02/15/94	01:06	GOES	Thin layer
02/17/94	01:06	GOES	Thin layer
03/04/94	01:06	GOES	Thin layer
03/08/94	01:09	NOAA 12	Two layers
03/17/94	01:09	GOES	Thin layer
03/26/94	00:06, 00:36, 01:06 and 01:36	GOES	Thick layer
04/07/94	00:22	NOAA 12	Thin layer
04/11/94	00:36	NOAA 12	Thick layer
04/15/94	00:49	NOAA 12	Two layers

LIST OF FIGURES

Figure 1: The physical thickness vs. the visible optical depth of semi-transparent clouds observed by the HSRL in 1993 and 1994.

Figure 2: Scatter plot of the visible and infrared optical depths measured by the combination of the HSRL lidar (visible optical depth at 0.53 μm) and NOAA and GOES satellite data (infrared 10.8 μm window channel). The diagonal line is a ratio of 2.0 (visible/IR). Error bars are shown on each data point.

Figure 3: Time-height image of the backscatter cross section $\beta_a(r) \frac{P(\pi,r)}{4\pi}$ (see Eq. 2) from the HSRL (upper panel). The lower panel is the visible optical depth integrated from 8.5 to 12 km altitude on 26 October 1993.

Figure 4: NOAA 12 1 km HRPT image from AVHRR Channel 4 (10.8 μm) from 26 October 1993. This image was remapped into an equal distant latitude-longitude projection. The location of the HSRL is indicated by the black dot.

Figure 5: Time-height image of the backscatter cross section $\beta_a(r) \frac{P(\pi,r)}{4\pi}$ (see Eq. 2) from the HSRL (upper panel). The lower panel is the visible optical depth integrated from 4 to 10 km altitude on 11 November, 1993. The extremely white layers between 5 and 5.5 km were liquid water as determined from depolarization measurements (not shown).

Figure 6: NOAA 12 1 km HRPT image from AVHRR Channel 4 (10.8 μm) from 11 November 1993. This image was remapped into an equal distant latitude-longitude projection. The location of the HSRL is indicated by the black dot.

Figure 7: Time-height image of the backscatter cross section $\beta_a(r) \frac{P(\pi,r)}{4\pi}$ (see Eq. 2) from the HSRL (upper panel). The lower panel is the visible optical depth integrated from 7 to 11 km altitude on 2 September, 1993.

Figure 8: NOAA 12 AVHRR Channel 4 infrared image from 2 September, 1993.

Figure 9: Time-height image of the backscatter cross section $\beta_a(r) \frac{P(\pi,r)}{4\pi}$ (see Eq. 2) from the HSRL (upper panel). The lower panel is the visible optical depth integrated from 3.5 to 11 km altitude on 15 April, 1994.

Figure 10: NOAA 12 AVHRR Channel 4 infrared image from 15 April, 1994.

Figure 11: The cross wind (top panel) and along the wind (bottom panel) images of range corrected backscatter from the Volume Imaging Lidar for 19:50 UT (13:50 CST) on 1 December 1989 at Madison, WI.

Figure 12: Same as Fig. 11 for 20:07 UT (15:07 CST) on 1 December 1989.

Figure 13: Error or difference in vertically integrated backscatter for an area vs. a line average, plotted as a function of separation distance between the locations of the area and line averaged volumes for the period of 19:30 to 20:30 UT, 1 December, 1989.

Figure 14: Same as Fig. 12 for the period, 20:30 to 21:30 UT, 1 December, 1989.

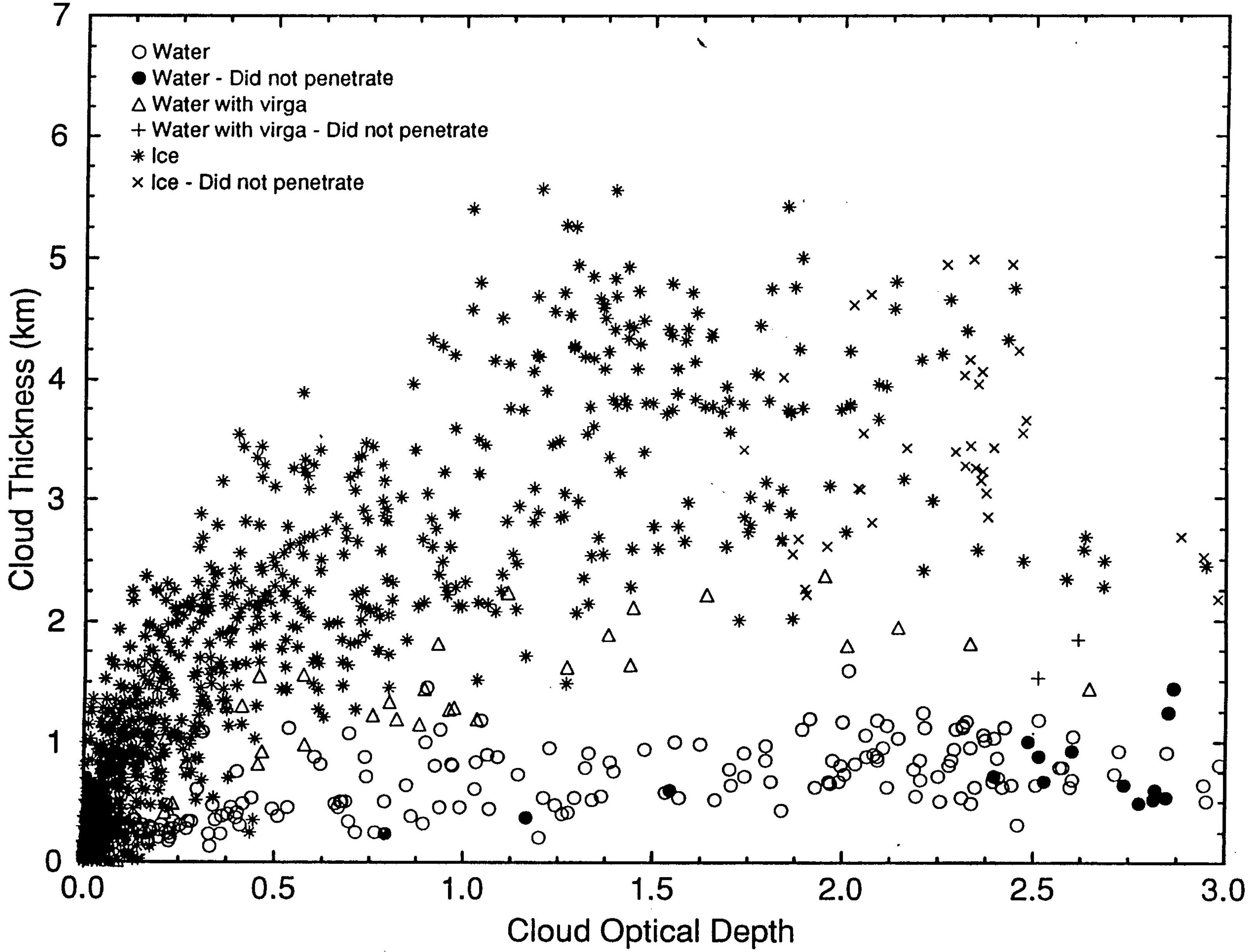

Figure 1: The physical thickness vs. the visible optical depth of semi-transparent clouds observed by the HSRL in 1993 and 1994.

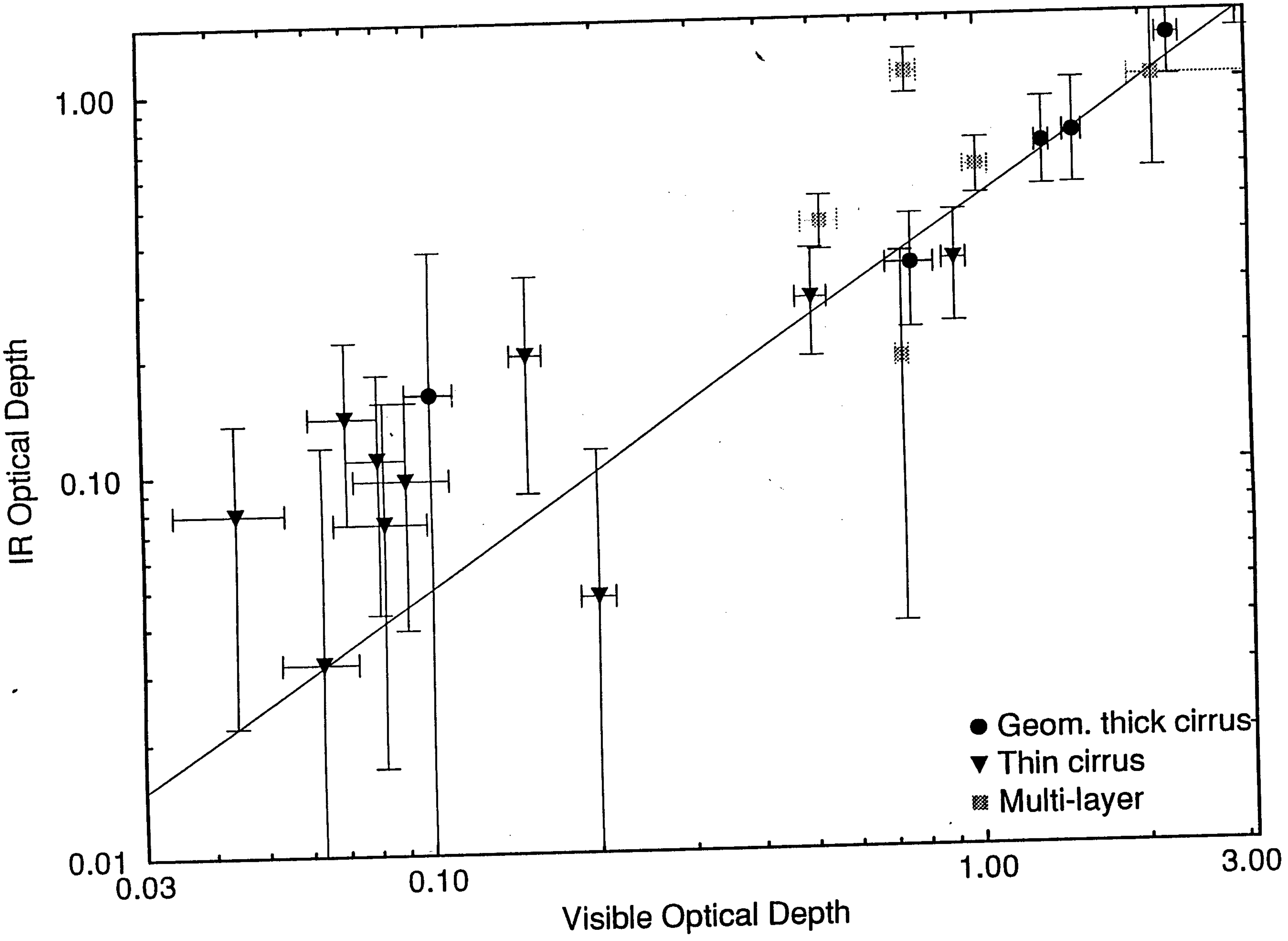

Figure 2: Scatter plot of the visible and infrared optical depths measured by the combination of the HSRL lidar (visible optical depth) and NOAA and GOES satellite data (infrared 10.8 μm window

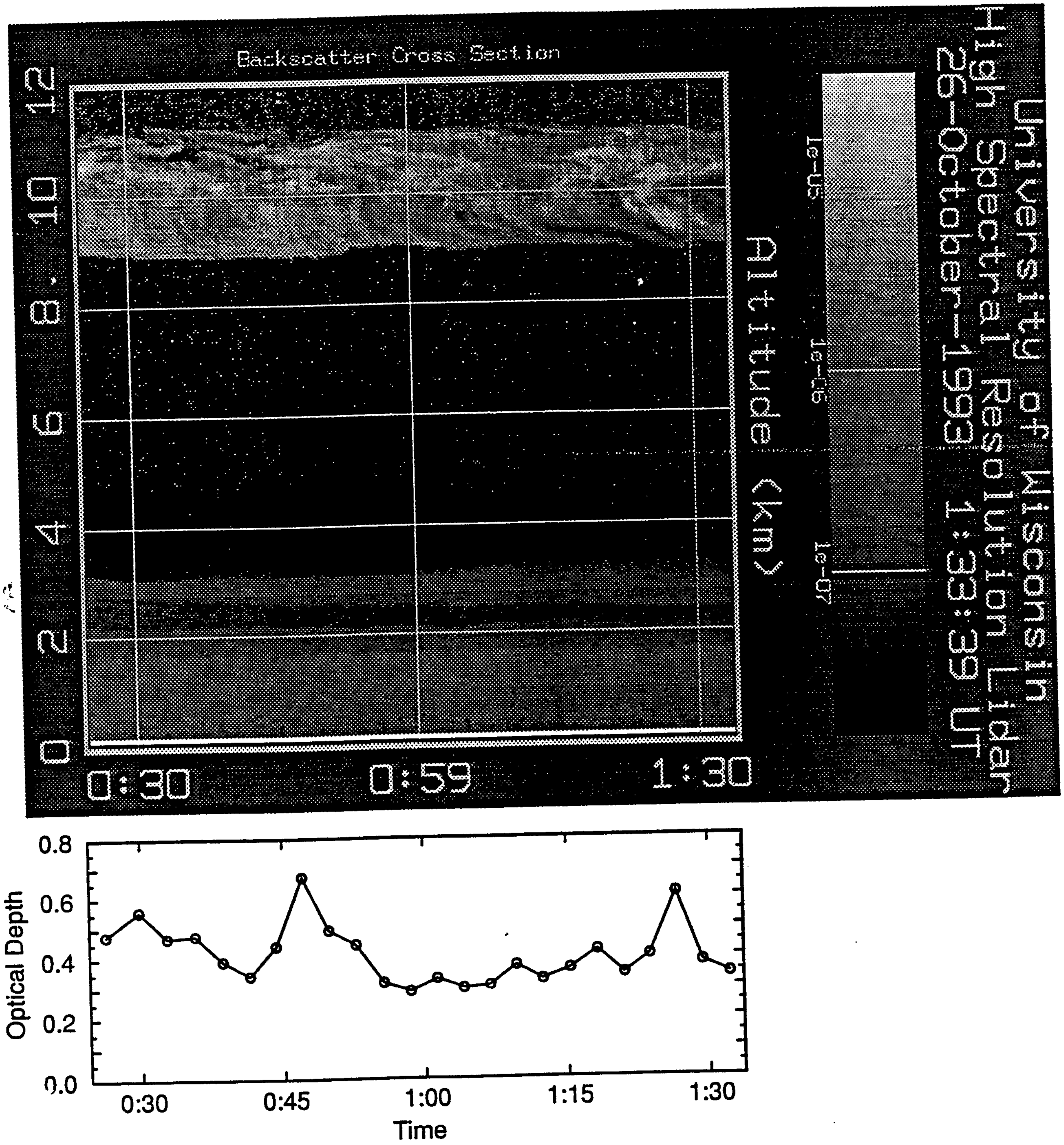

Figure 3: Time-height cross section of backscatter (upper panel) and visible optical depths between 8.5 and 12 km (lower panel) from the HSRL on 26 October 1993.

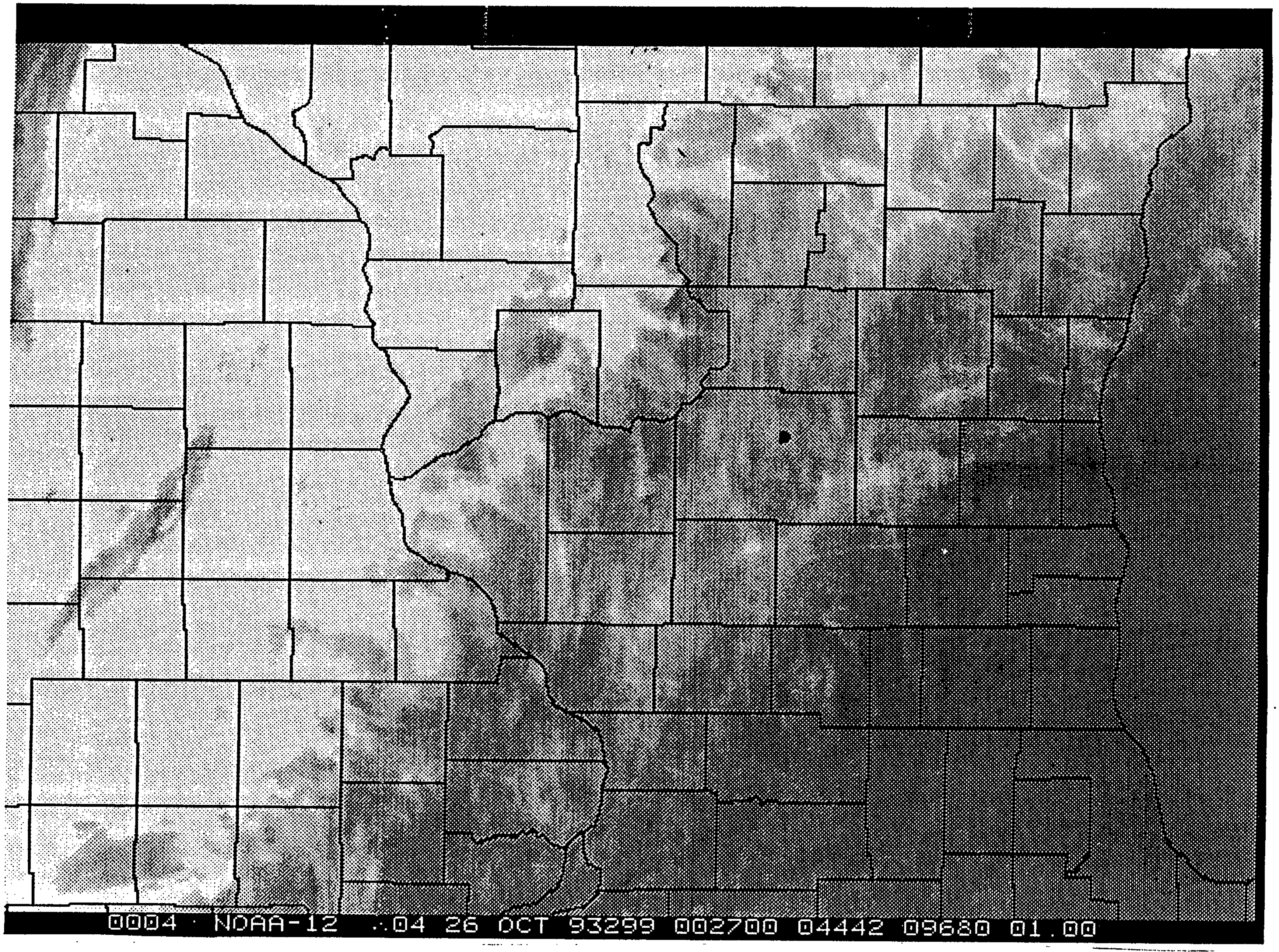

Figure 4: NOAA 12 1 km HRPT image from AVHRR Channel 4 (10.8 μm) from 26 October 1993. This image was remapped into an equal distant latitude-longitude projection. The location of the HSRL is indicated by the black dot.

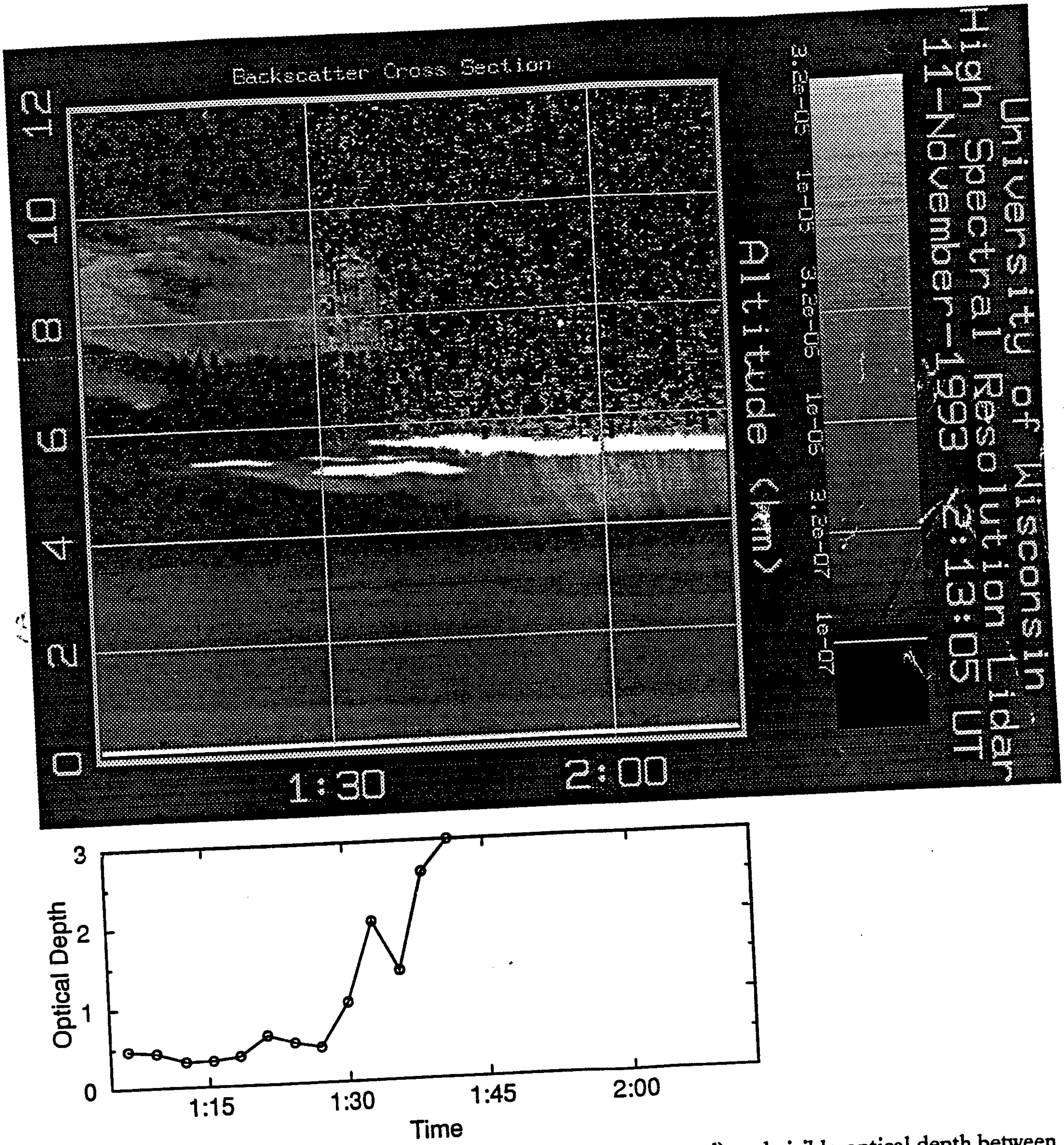

Figure 5: Time-height cross section of backscatter (upper panel) and visible optical depth between 4 and 10 km from the HSRL on 11 November 1993. The extremely white layers between 5 and 5.5 km were liquid water as determined from depolarization measurements (not shown).

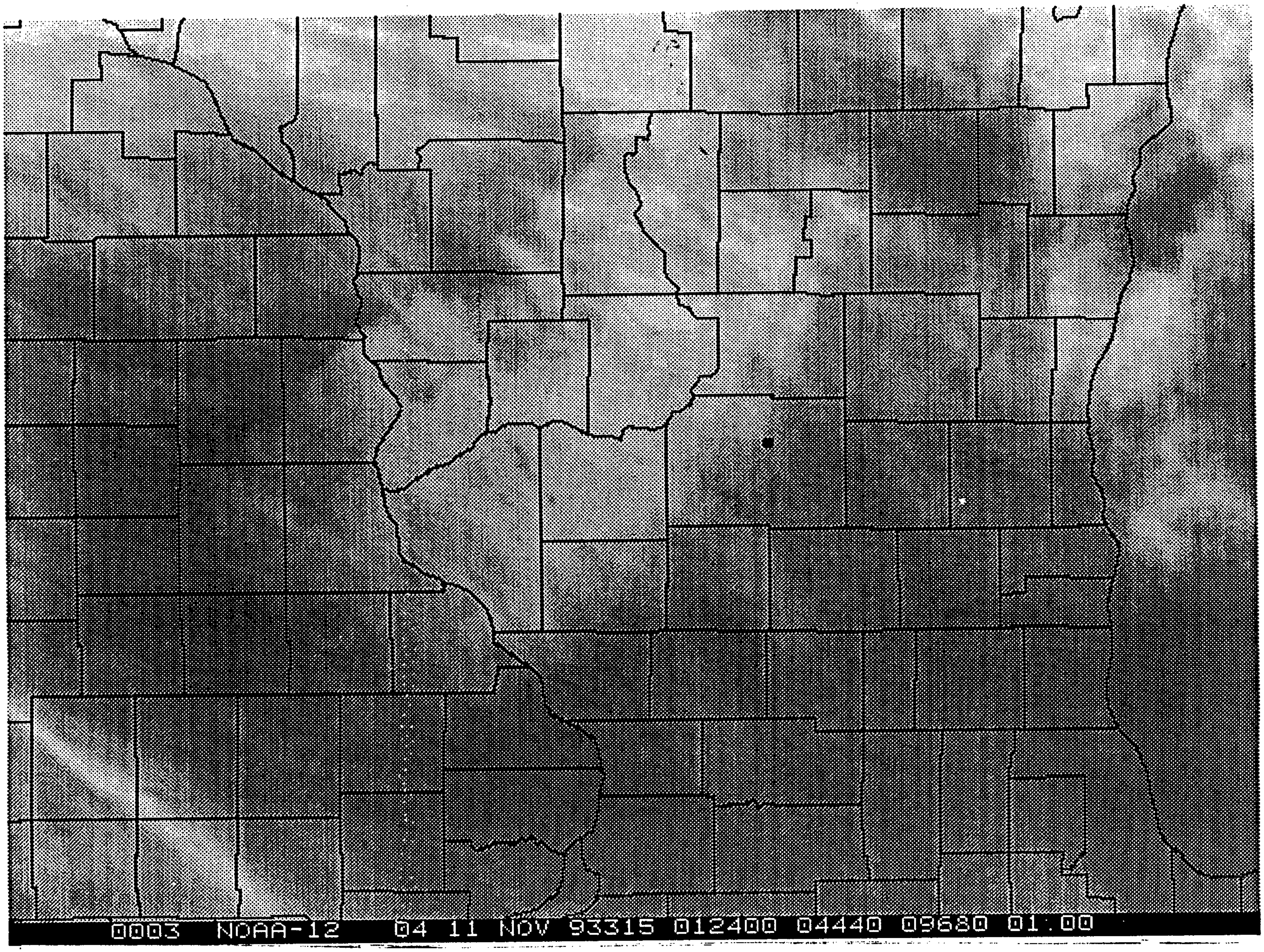

Figure 6: NOAA 12 1 km HRPT image from AVHRR Channel 4 (10.8 μm) from 11 November 1993. This image was remapped into an equal distant latitude-longitude projection. The location of the HSRL is indicated by the black dot.

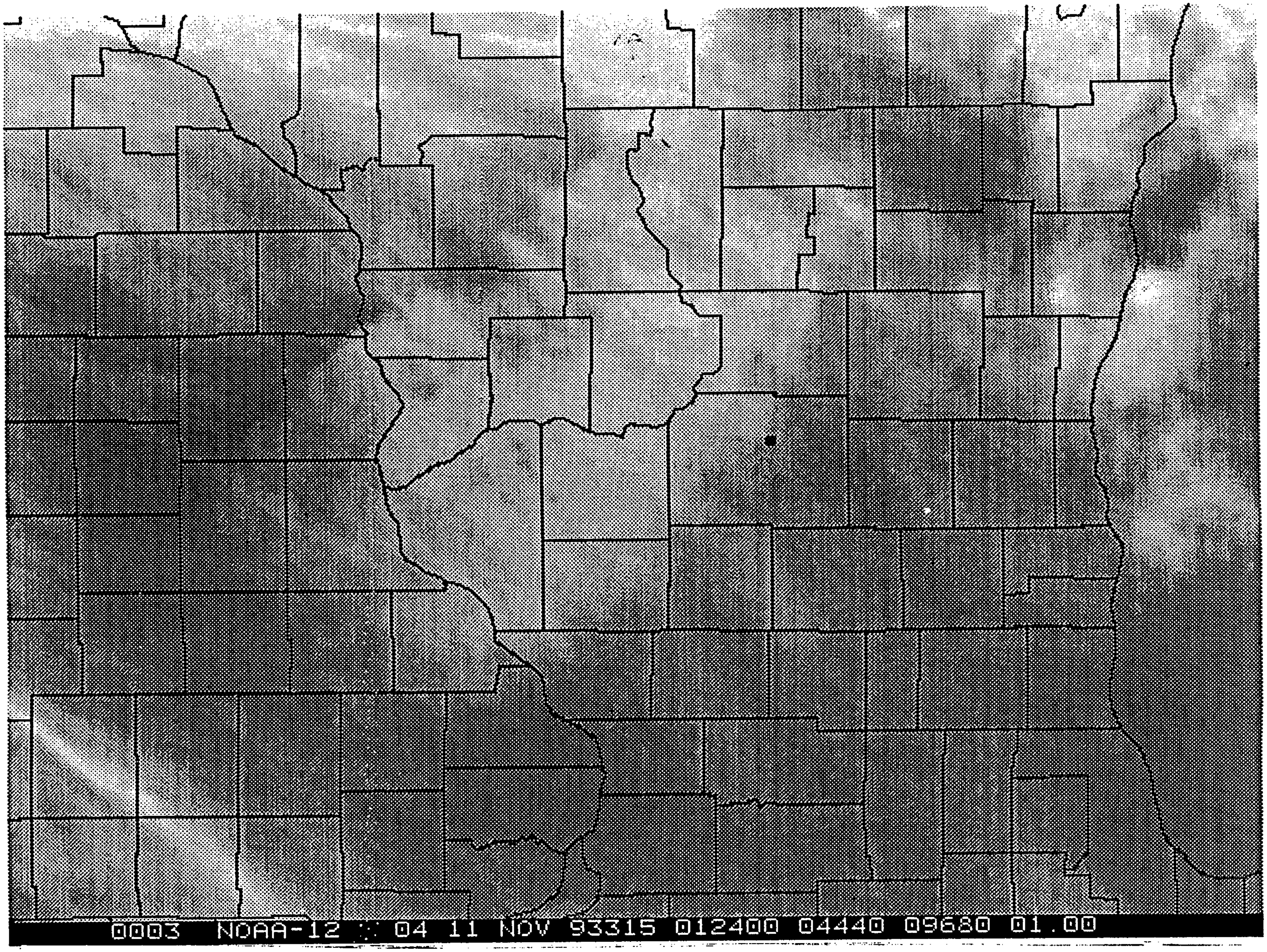

Figure 6: NOAA 12 1 km HRPT image from AVHRR Channel 4 (10.8 μm) from 11 November 1993. This image was remapped into an equal distant latitude-longitude projection. The location of the HSRL is indicated by the black dot.

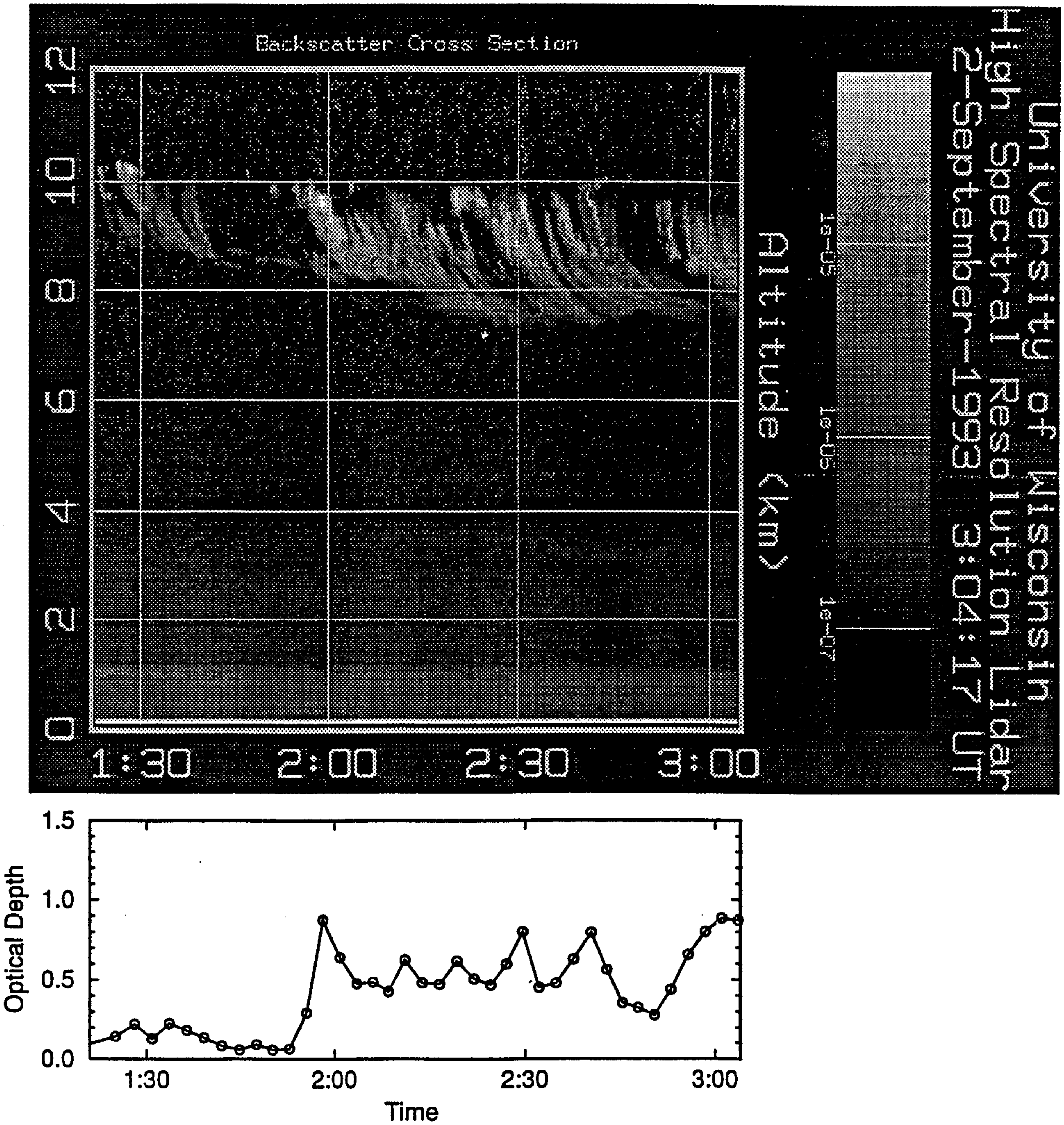

Figure 7: Time-height cross section of backscatter (upper panel) and visible optical depth between 7 and 11 km (lower panel) from 2 September, 1993, measured by the HSRL.

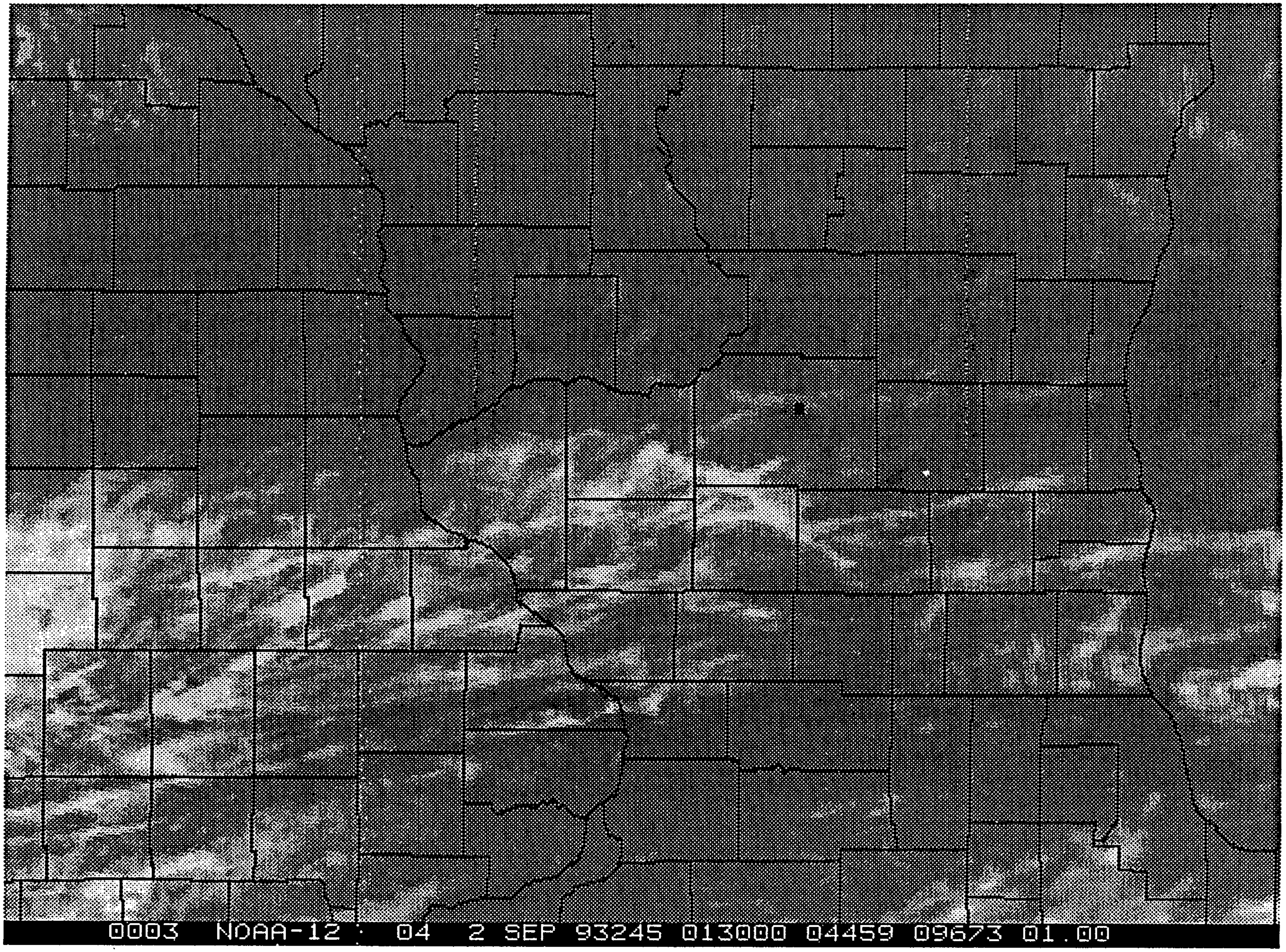

Figure 8: NOAA 12 AVHRR Channel 4 infrared image from 2 September, 1993.

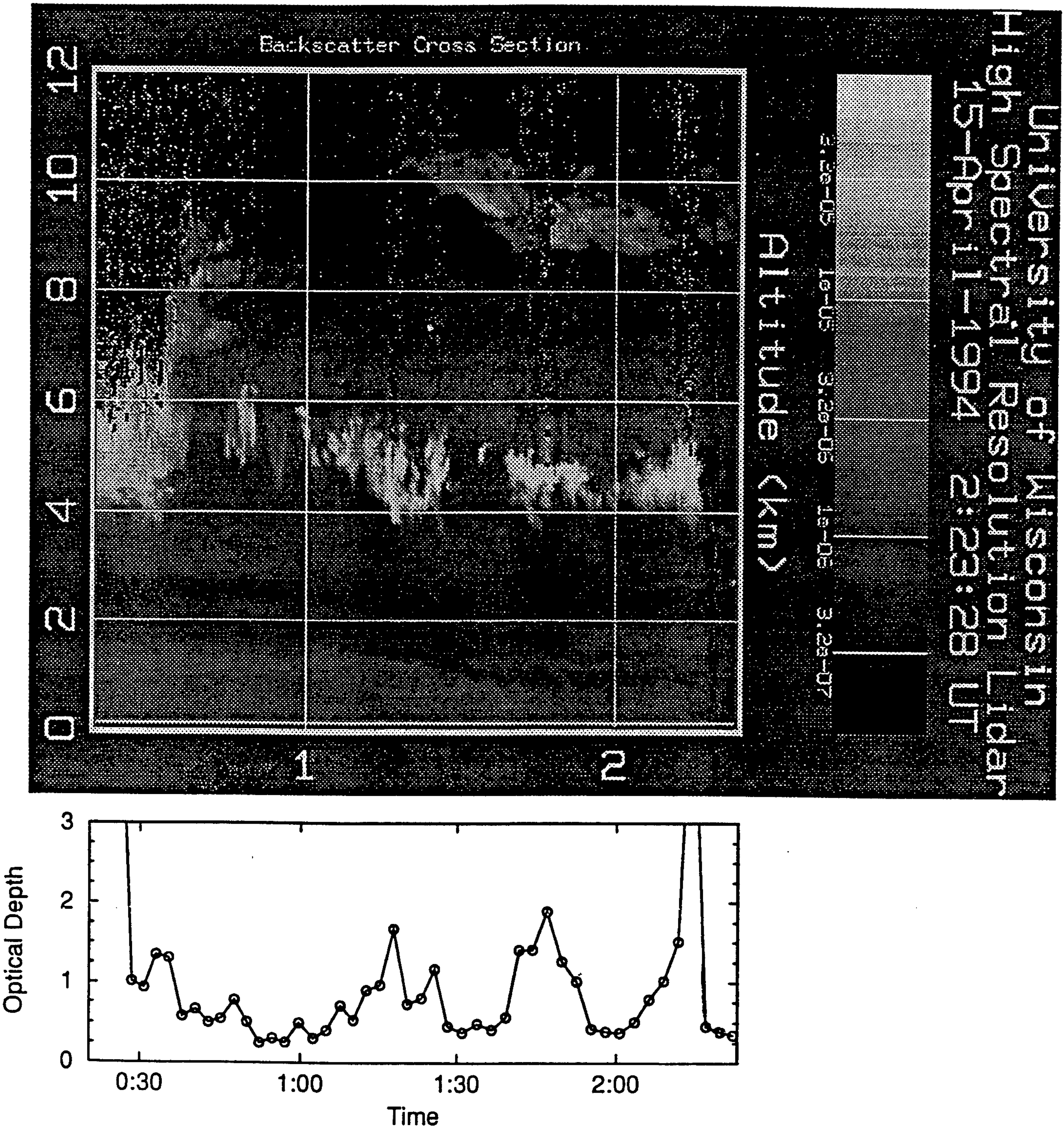

Figure 9: Time-height cross section of backscatter (upper panel) and visible optical depth between 3.5 and 11 km (lower panel) from 15 April, 1994, measured by the HSRL.

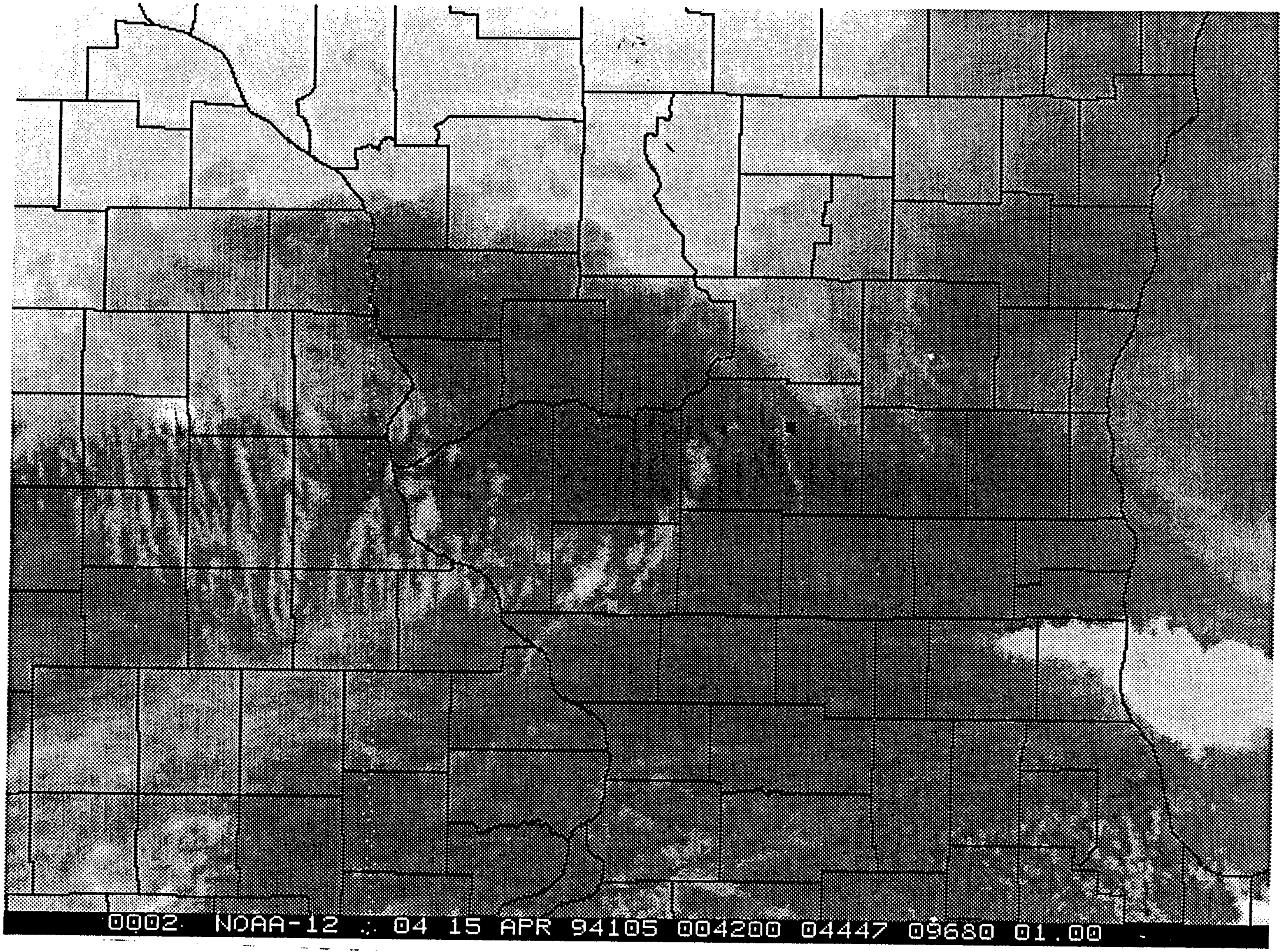

Figure 10: NOAA 12 AVHRR Channel 4 infrared image from 15 April, 1994.

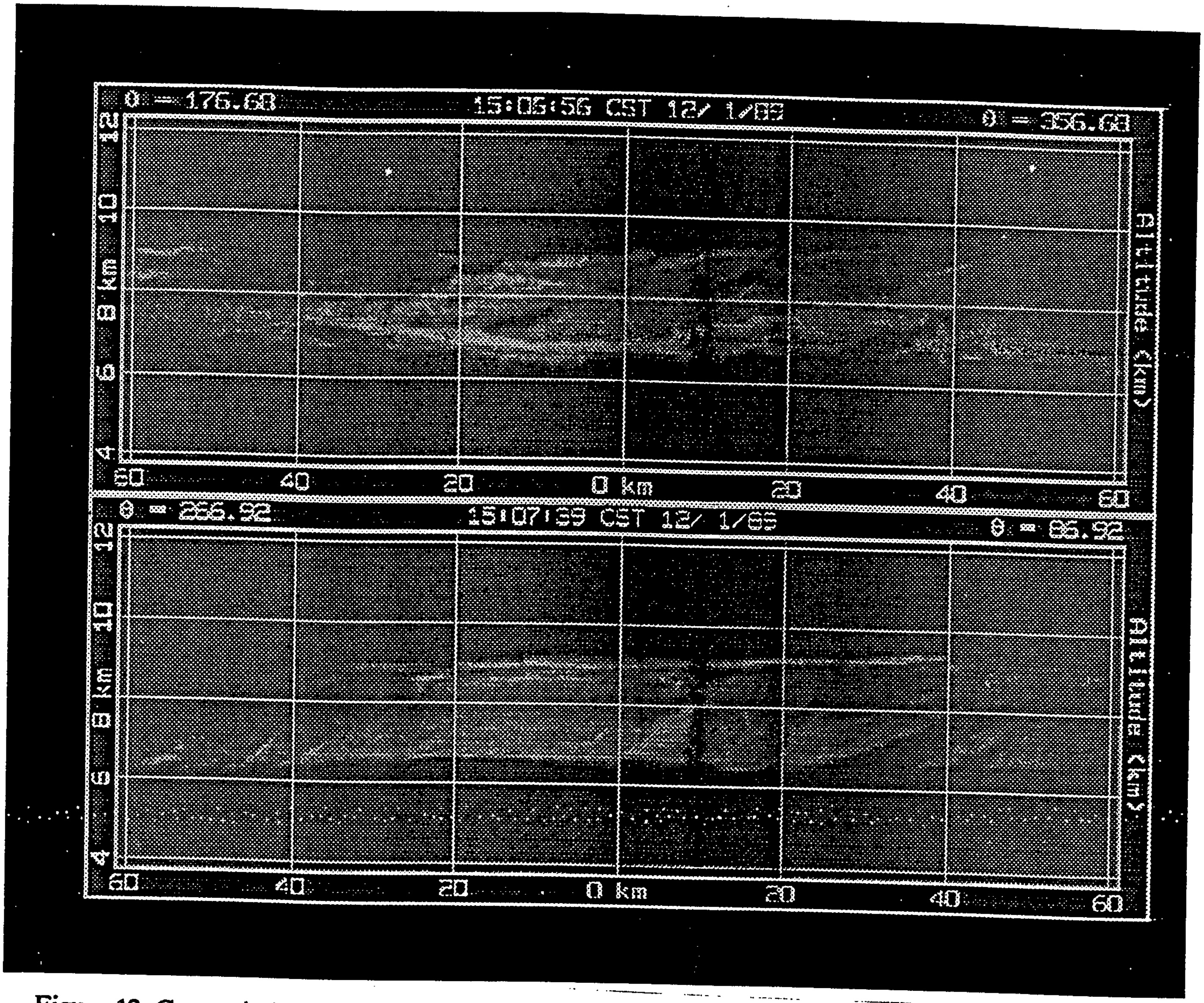

Figure 12: Cross wind (top panel) and along the wind (bottom panel) cross sections from the Volume Imaging Lidar backscatter data at 20:07 UT (15:07 CST) on 1 December 1989.

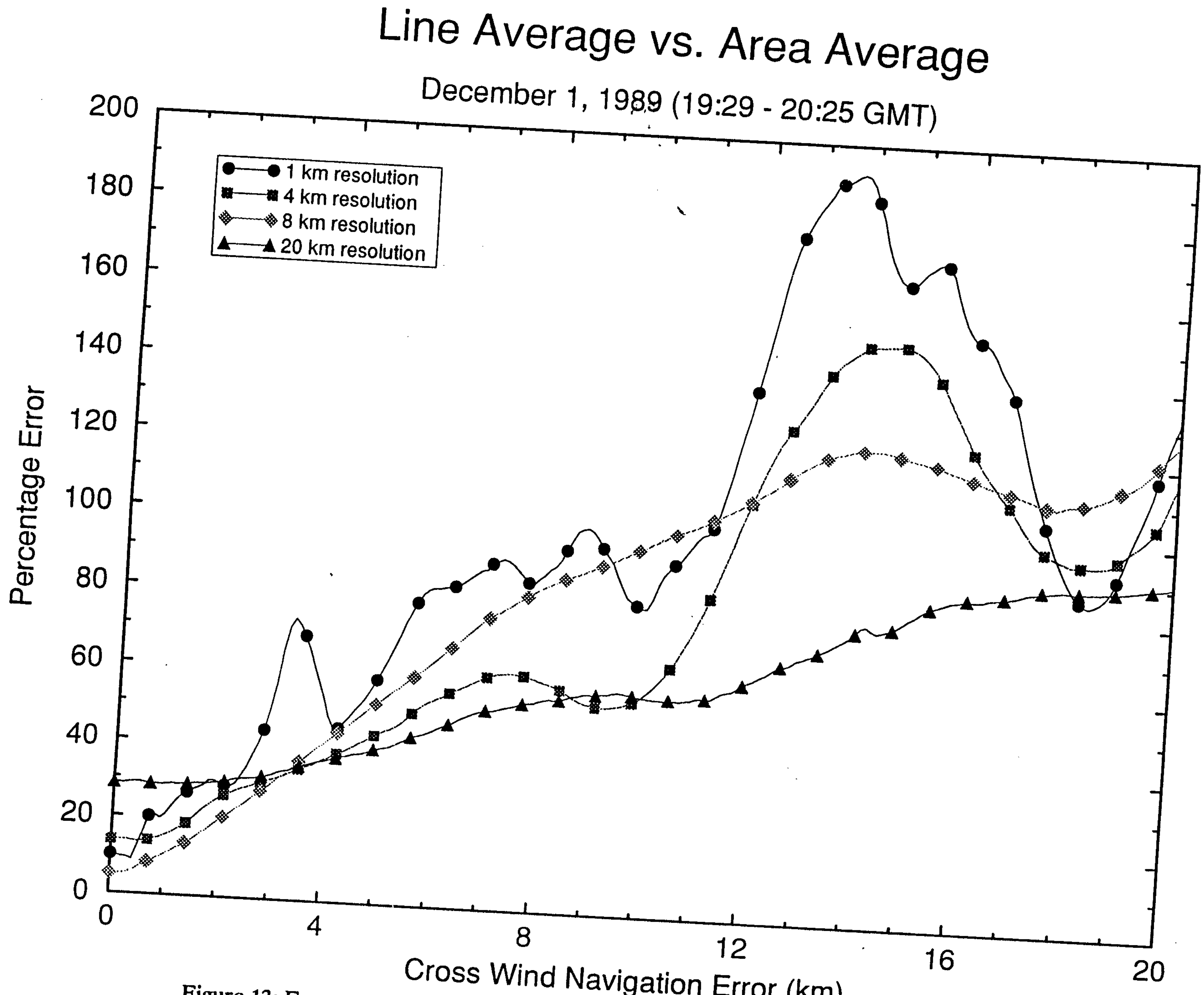

Figure 13: Error or difference in vertically integrated backscatter averages for an areal vs. a line average plotted as a function of separation distance (Along Wind Navigation Misalignment) in the along the wind direction for the period of 19:30 to 20:30 UT, 1 December, 1989.

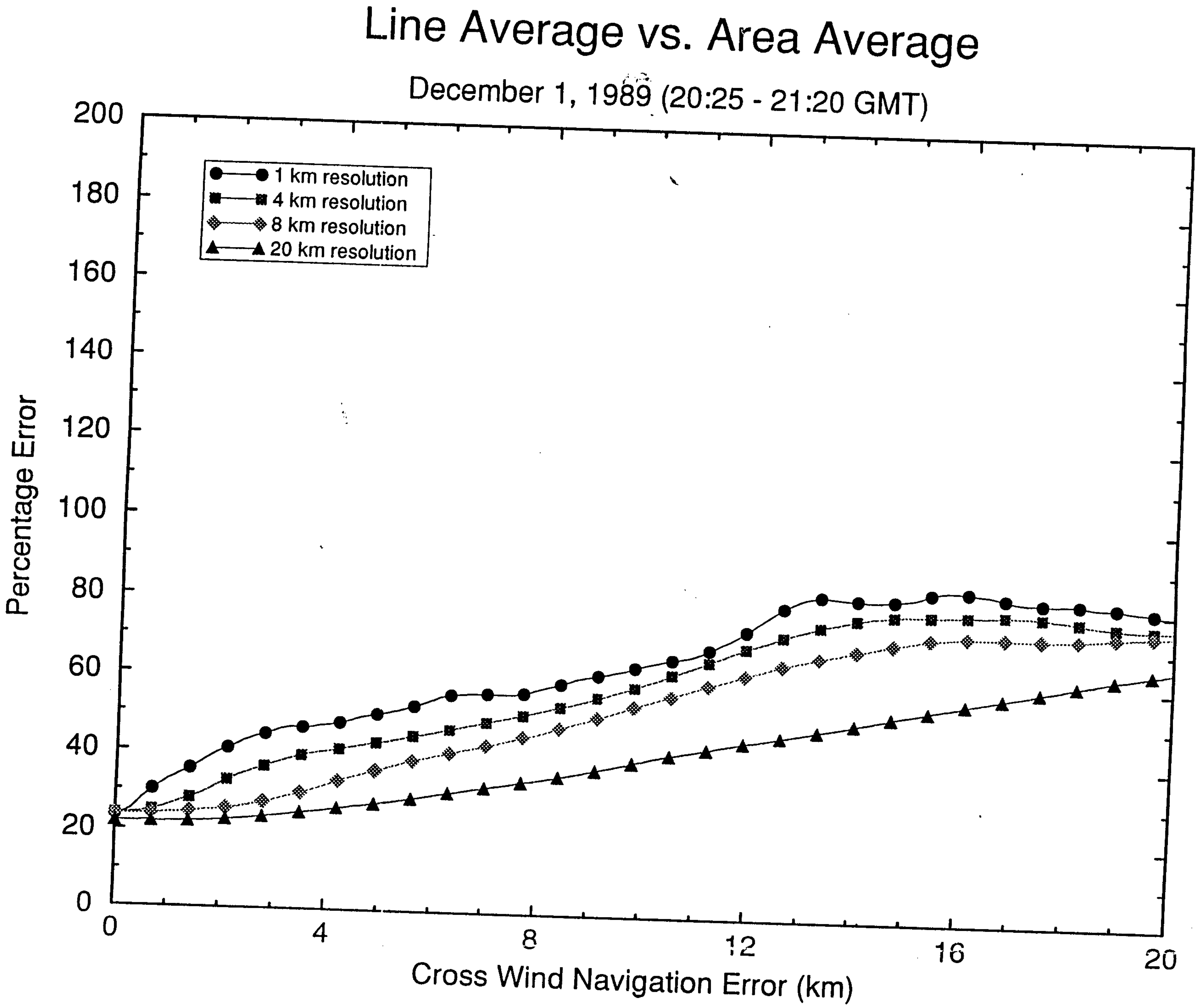

Figure 14: Same as Fig. 12 for the period, 20:30 to 21:30 UT, 1 December, 1989.